Antioxidant activity and cellular response of novel cerium oxide nanoparticles stabilized with triethylene glycol under H_2O_2 stress in fibroblasts and keratinocytes

Viktoriia A. Anikina[1]*, Daniil A. Kozlov[2], Anton L. Popov[3], Elizaveta A. Zamyatina[1], and Nelli R. Popova[1]*

ABSTRACT

Oxidative stress has been demonstrated to play a key role in the process of skin injury and delayed wound healing. Consequently, the development of effective antioxidant nanomaterials has been identified as a promising strategy for dermatological applications. In this study, we synthesized ultra-small cerium oxide nanoparticles stabilized with triethylene glycol (CeNPs@TEG) using a single-step synthesis. We synthesized cerium oxide nanoparticles (CeNPs) with a size of 3 nm and a hydrodynamic diameter of 13 nm. The elevated triethylene glycol (TEG) content facilitated the formation of a stable sol without the necessity of additional surfactants, thereby preserving the surface activity of the CeNPs. The antioxidant activity of CeNPs@TEG was assessed using hydrogen peroxide (H_2O_2) as a representative reactive oxygen species (ROS), chosen for its stability and regulatory role in skin repair processes. At micromolar concentrations, CeNPs@TEG efficiently scavenged H_2O_2 in buffer solution, demonstrating strong ROS-neutralizing capacity. The cytotoxicity was evaluated in human fibroblasts and keratinocytes using MTT and Live/Dead assays. This confirmed the high level of biocompatibility and negligible effect on cell viability and activity of the reduced form of nicotinamide adenine dinucleotide phosphate (NADP-H)-dependent oxidoreductases. Pre-incubation of cells with CeNPs@TEG for 24 h prior to H_2O_2-induced oxidative stress exposure led to a significant reduction in intracellular ROS levels and enhanced activity of NADP-H-dependent oxidoreductases, indicating cytoprotective effects. The findings demonstrate that CeNPs@TEG combine an ultra-small size, high stability, low toxicity, and effective ROS scavenging, supporting their potential use in therapeutic strategies aimed at protecting skin cells from oxidative damage and enhancing wound healing.

Keywords:
Biomedical application; Cerium oxide nanoparticles; Human fibroblasts; Human keratinocytes; Oxidative stress; Triethylene glycol

***Corresponding authors:**
Viktoriia A. Anikina,
anikinava@iteb.pushchino.ru;
Nelli R. Popova,
popovanr@iteb.pushchino.ru

How to cite this article:
Anikina, V.A.; Kozlov, D.A.; Popov, A.L.; Zamyatina, E.A.; Popova, N.R. Antioxidant activity and cellular response of novel cerium oxide nanoparticles stabilized with triethylene glycol under H_2O_2 stress in fibroblasts and keratinocytes. *Biomater Transl.* 2025.

doi: 10.12336/bmt.25.00047

1. Introduction

Reactive oxygen species (ROS) play an important role in skin regeneration. At physiologically acceptable concentrations, they are involved in activating cellular signaling pathways that promote cell proliferation and migration. They also stimulate angiogenesis by inducing vascular endothelial growth factor and regulate the inflammatory response, facilitating the transition from inflammation to the regenerative phase of wound healing.[1,2] In addition, ROS plays a role in cell-mediated defense by activating macrophages, which helps prevent secondary infections during wound healing.[3-5] At the same time, excessive production of ROS, including singlet oxygen ($^1O_2$), superoxide anion ($\bullet O_2^-$), hydroxyl radical ($\bullet HO$), and the non-radical hydrogen peroxide

(H_2O_2), can lead to the formation of free radicals and the development of oxidative stress. This can trigger apoptosis and necrosis, increase the inflammatory response, and activate matrix metalloproteinases.[6,7] These processes slow down healing and can lead to chronic skin damage.

Ionizing radiation occupies a special place among exogenous factors that increase ROS levels. Its use in radiation therapy for cancer can lead to direct cellular damage and an inflammatory response in the skin.[8] It can also cause indirect damage through oxidative stress resulting from ROS formation during water radiolysis.[9-11] Exposure to ionizing radiation can cause a range of adverse skin reactions, including telangiectasia, alopecia, and radiation dermatitis.[12-14] Thus, eliminating pathologically high levels of ROS at the site of skin injury could be a promising and effective approach to enhancing skin regeneration. This is particularly relevant for radiation-induced skin damage, for which there are no universal therapeutic agents.

We consider the development of new biologically active nanomaterials that can modulate the level of ROS and accelerate wound healing to be highly important. Currently, cerium oxide nanoparticles (CeNPs) are among the most promising materials for use in regenerative medicine. CeNPs have low cytotoxicity, good biocompatibility, and high bioavailability, as well as strong antioxidant activity.[15-18] It has been shown that CeNPs possess unique physical and chemical properties, acting as an inorganic antioxidant that mimics several oxidoreductases, such as catalase, superoxide dismutase, and oxidase.[19-21] CeNPs inhibit intracellular oxidative stress by directly inactivating ROS and indirectly by modulating gene expression. This provides a natural and supportive environment for cell proliferation and migration. CeNPs also have antibacterial,[22] radioprotective,[23] regenerative, and wound healing properties.[24] In numerous studies, it has been demonstrated that as the size of CeNPs decreases, their biological activity increases, including in the treatment of skin injuries.[25-27] To decrease the size of CeNPs and increase their bioavailability, we propose synthesizing nanoparticles (NPs) by alkaline precipitation in a polyol solution. A suitable polyol may be triethylene glycol (TEG), which has low toxicity, anti-inflammatory activity, as well as disinfectant and moisturizing effects, and is used in ointments and gels for topical application.[28-31] Therefore, a glycolic solution of ultra-small size NPs or cerium oxide clusters could provide a ready-to-use formulation for the topical treatment of skin injuries.

In this study, we synthesized new CeNPs stabilized with TEG (CeNPs@TEG) and performed their comprehensive characterization. We also evaluated their cytotoxicity and biocompatibility against human fibroblast and keratinocyte cell cultures, as well as their antioxidant activity in aqueous buffer solutions and on cell cultures.

2. Methods

2.1. Synthesis of CeNPs@TEG

The following chemicals were used for preparing CeNPs@TEG: cerium (III) chloride heptahydrate (Alfa Aesar, United States of America [USA]); TEG (Sigma-Aldrich, USA); potassium hydroxide (Sigma-Aldrich, USA). For the synthesis of CeNPs@TEG, 80 mL of TEG and 3.8 g of cerium chloride heptahydrate were placed in a glass beaker, heated to 50°C, and stirred on a magnetic stirrer for 2 h at 500 rpm until completely dissolved. After that, the resulting solution was cooled in the refrigerator at 4–8°C. In a separate container, 1.9 g of potassium hydroxide (KOH) was dissolved in 2 mL of deionized water, after which 10 mL of TEG was added. The solution was stirred on a magnetic stirrer until transparent without heating. A glass with a solution of cerium salt was placed on a magnetic stirrer, and a prepared solution of potassium hydroxide with TEG was quickly poured into it. As a result, the color of the solution changed from colorless to black–brown (transparent solution in a thin layer), and a glycol solution of ultra-small CeNPs was obtained. The resulting CeNPs@TEG was left on a magnetic stirrer at 300 rpm at room temperature for 24 h.

We tested different amounts of KOH to evaluate their influence on the pH of the medium and NP formation. For instance, when 2.2 g of KOH was used, the pH value was 11.15 after 24 h, gradually decreasing to 9.64 after 72 h. Under these conditions, larger NPs (>30 nm) were observed, and colloidal stability was reduced. At lower KOH concentrations (1.6 g), the initial pH values were in the range of 7.2, dropping to 6.2–6.4 after 72 h. This resulted in the incomplete formation of CeNPs or unstable sols. In contrast, under optimized conditions (1.9 g of KOH dissolved in 2 mL of H_2O and mixed with 10 mL of TEG before being added to the cerium salt solution), the pH increased temporarily to ~12.0 immediately after mixing, stabilizing at ~7.5 after 24 h.

2.2. Characterization of CeNPs@TEG

Transmission electron microscopy (TEM) images and selected area electron diffraction patterns were acquired using a charge-coupled device camera (Ultra Scan 4000, Gatan, USA) installed in a transmission electron microscope (Zeiss Libra 200MC, Zeiss, Germany) operated at 200 kV. The hydrodynamic diameter and ζ-potential of the NPs were determined using a zeta particle size analyzer (BeNano, BetterSize, China) through dynamic and electrophoretic light scattering techniques. Infrared spectra were recorded with a Fourier-transform spectrometer (FSM 2202, Infraspek, Russia) over the 400–4000 cm^{-1} range at a resolution of 2 cm^{-1}, employing diffuse reflectance mode with a standard sample holder. The optical absorption spectra were measured in the wavelength range 200–800 nm with 1 nm resolution using a spectrophotometer (SF-2000, OKB Spectrum, Russia).

[1]Isotope Research Laboratory, Institute of Theoretical and Experimental Biophysics of the Russian Academy of Sciences, Pushchino, Moscow Oblast, Russia; [2]Nanobiomaterials and Bioeffectors for the Theranostics of Socially Significant Diseases Laboratory, Kurnakov Institute of General and Inorganic Chemistry of the Russian Academy of Sciences, Moscow, Russia; [3]Theranostics and Nuclear Medicine Laboratory, Institute of Theoretical and Experimental Biophysics of the Russian Academy of Sciences, Pushchino, Moscow Oblast, Russia

2.3. Assessment of the antioxidant activity of CeNPs@TEG

For the assessment of CeNPs@TEG antioxidant activity, a highly sensitive enhanced chemiluminescence method was used in the "luminol-4-iodophenol-horseradish peroxidase" system. This system enables the quantification of the concentration of H_2O_2 in aqueous solutions. The chemiluminescence intensity was measured using a Beta-1 liquid scintillation counter (Medical Equipment, Ukraine) operating in the single photon counting mode (without a coincidence scheme).[32]

Experimental samples were prepared in 20-mL glass vials (Beckman, USA) using phosphate-buffered saline (PBS) (PanEko, Russia) at pH values of 5.5, 6.8, and 7.4. H_2O_2 (Sigma-Aldrich, USA) was then added to a concentration of 1200 nM in the solution, after which the samples were incubated for an hour. To minimize the effect of viscosity in the TEG solution, a modification of the method for measuring viscous solutions was used.[33] After the incubation samples (300 µl) were placed in polypropylene tubes (Eppendorf, Germany) and 300 µL of a freshly prepared "counting solution" containing tris-(hydroxymethyl)-aminomethane (Sigma-Aldrich, USA) pH 8.5, 4-iodophenol (Sigma-Aldrich, USA), luminol (PanReac Applichem, Germany) in a ratio of 40:1.2:1 and 0.3–0.7 µL of a concentrated horseradish peroxidase solution (Sigma-Aldrich, USA) was added. All procedures were performed under low-light conditions.

The final concentration of H_2O_2 in the solution was determined using a calibration curve. The concentration of the H_2O_2 solution used for the calibration was measured spectrophotometrically at λ = 240 nm using a known molar absorption coefficient of 43.6 $M^{-1} \times cm^{-1}$ on the DeNovix DS-11 + spectrophotometer (DeNovix, USA).

2.4. Cell culture

Human fibroblasts (HF) and human keratinocytes (HaCaT) were obtained from the cryostorage of the Theranostics and Nuclear Medicine Laboratory (ITEB RAS, Russia). HF and HaCaT were cultured in Dulbecco's Modified Eagle's Medium F12 (PanEko, Russia) (1:1) and Dulbecco's Modified Eagle's Medium – high glucose (PanEko, Russia) (1:1), respectively, medium with the addition of 10% fetal bovine serum (Global Kangqin Huangdao Biotechnology Co, China) and 100 U/mL penicillin/streptomycin (PanEko, Russia) under 5% CO_2 at 37°C.

2.5. 3-[4,5-dimethylthiazol-2-yl]-2,5-diphenyl tetrazolium bromide (MTT) assay

Cellular reduced form of nicotinamide adenine dinucleotide phosphate (NADP-H)-dependent oxidoreductase activity was assessed using the MTT assay. This assay relies on the enzymatic reduction of the water-soluble MTT salt (PanEko) to an insoluble purple formazan product. Cells were plated in 96-well plates at a density of 30,000 cells/cm^2. After 24, 48, and 72 h of incubation with CeNPs@TEG at concentrations ranging from 25 to 1000 µM, the culture medium was replaced with MTT solution (0.5 mg/mL in DMEM/F12) or DMEM. Following 3 h of incubation, the MTT-containing medium was removed, and dimethyl sulfoxide (PanEko) was added to solubilize the formazan crystals. Plates were gently agitated on a plate shaker for 10 min to ensure complete dissolution, and absorbance was recorded at 540 nm using a plate reader (Multiskan FC, Thermo Fisher Scientific, USA). Data were normalized to control wells and presented as mean ± standard deviation (SD).

2.6. Live/dead assay

Cell viability after exposure to CeNPs@TEG was assessed using a fluorescent cell imager (ZOE, BioRad, USA). Cells were seeded into 96-well plates at a density of 30,000 cells/cm^2 and stained with Hoechst 33342 (Lumiprobe, Russia) fluorescent dye (absorption: 350 nm, emission: 461 nm) and a propidium iodide dye (Lumiprobe, Russia) (absorption: 493 nm, emission: 636 nm). The dyes were added to the culture medium without serum (1 µg/mL), and the plate was placed in a CO_2 incubator (RWD Life Science, China) for 15 min under 5% CO_2 at 37°C. Microphotographs were taken after washing the cells with PBS. For each cell group, five fields in each well were examined. The number of cells (total cells/dead cells) was calculated using the ImageJ 1.54h software (National Institutes of Health, USA).

2.7. Hydrogen peroxide-induced oxidative stress *in vitro*

The protective action of CeNPs@TEG was analyzed using an experimental model of oxidative stress, whereby the cells were treated with 200 µM H_2O_2 (Sigma-Aldrich, USA). Samples were added to the cell culture, then 24 h later, the cells were treated with H_2O_2 for 60 min. At the end of the incubation period, cytotoxicity tests were performed, including the MTT assay and the Live/Dead assay, as well as measurements of intracellular ROS levels.

2.8. Intercellular ROS analysis

Intracellular ROS levels were measured using 6-carboxy-2',7'-dichlorodihydrofluorescein diacetate (6-carboxy-H_2DCFDA) (Lumiprobe, Russia). The 6-carboxy-H_2DCFDA is a non-fluorescent compound that begins to fluoresce when it is cleaved by cellular esterases, releasing the acetyl groups, and becomes oxidized within the cell. The resulting product, 6-carboxy-2',7'-dichlorofluorescein, has a bright green fluorescence (λ_{ex} = 511 nm, λ_{em} = 533 nm). After 24, 48, or 72 h, the culture medium containing the tested substances was replaced with 6-carboxy-H_2DCFDA solution at 10 µM concentration, then the cells were washed twice with Hanks' balanced salt solution (PanEko, Russia). The analysis of the cells was immediately carried out using a microplate reader (Biotek Synergy H1, Agilent Technologies, USA). The fluorescence intensity values were recalculated as percentages of the control group.

2.9. Statistical Analysis

The experimental data are presented as the mean ± SD. The statistical significance of differences between the values in experimental groups was determined using Student's and Welch's *t*-tests. Differences were considered statistically significant at $0.01 \le p < 0.05$ (*), $0.001 \le p < 0.01$ (**).

3. Results

3.1. Characterization of CeNPs@TEG

We synthesized CeNPs@TEG through a single-step approach, following the synthesis protocol described in the methods section. **Figure 1** illustrates the synthesis process and the proposed chemical structure of CeNPs@TEG. **Figure 2** presents the physicochemical characteristics of the CeNPs@TEG. According to TEM data, a glycolic sol of crystalline CeNPs with a size of 3.2 ± 0.7 nm was synthesized (**Figure 2A**). The obtained NPs were well crystallized based on the high-resolution TEM image (**Figure 2B**) and electron diffraction pattern (**Figure 2C**) corresponding to the cerium oxide structure. It was found that the hydrodynamic diameter of CeNPs in the sol was 13 nm (**Figure 2E**). Measurements by electrophoretic light scattering techniques indicated that the ζ-potential of CeNPs@TEG was +1.48 mV (**Figure 2F**). The results of infrared spectroscopy for CeNPs@TEG compared with TEG and with the reaction mixture of TEG with cerium chloride are shown in **Figure 2G**. The infrared spectra of all samples were highly similar, displaying only absorption bands corresponding to TEG, which could be attributed to its excess in the CeNPs@TEG sol obtained. In the spectra, the absorption bands around 3500 cm^{-1} were assigned to water. The regions of 2970–2870 cm^{-1} and 1480 cm^{-1} corresponded to the stretching and bending modes of $–CH_2–$ groups, respectively. The band at 1150 cm^{-1} arose from the stretching mode of –C–O–C– bonds. The absorption spectrum of TEG showed no distinct bands in the 200–800 nm range. However, after adding a cerium chloride solution to TEG, the absorption spectrum changed significantly. The spectrum displayed four intense absorption bands near 210, 220, 238, and 250 nm, along with a weak peak at 295 nm, which are characteristic of Ce^{3+} complexes, confirming the retention of cerium in the +3 oxidation state. In contrast, the absorption spectrum of the CeNPs@TEG sol differs markedly, showing a strong absorption edge at wavelengths below 400 nm, indicative of CeO_2 NPs formation.

The colloidal stability of CeNPs@TEG was assessed using dynamic light scattering techniques. After 9 months, the average particle size was 6.2 ± 2.2 nm, and after 18 months, it was 6.3 ± 0.9 nm, confirming minimal aggregation over prolonged storage. This indicates that polyglycols provide high stability for CeO_2 NPs.

3.2. Antioxidant activity of CeNPs@TEG

As mentioned earlier, a pathological increase in ROS levels results in slowed skin healing and the maintenance of chronic inflammation at the site of injury. H_2O_2 is a major secondary messenger in wound healing processes and one of the longest-lived forms of ROS. Therefore, in this study, we modeled oxidative stress by adding a fixed amount of H_2O_2 to PBS (1 mM) with different pH values. The pH range was chosen based on data from human skin physiology and the redox potential of CeNPs@TEG, which depends on the pH of the environment. Data were collected for pH values of 5.5, 6.8, and 7.4, as shown in **Figure 3**.

It was found that CeNPs@TEG exhibited antioxidant properties in a concentration range from 25 μM to 250 μM. The highest effective concentration at all pH values studied in this system was 125 μM. At 125 μM, as the pH increased, the addition of CeNPs@TEG to the system resulted in a reduction of exogenous H_2O_2 by 90–100%. At 50 μM, a significant dependence of CeNPs@TEG antioxidant activity on pH was observed: at pH 5.5, exogenous H_2O_2 levels decreased by 7% (**Figure 3A**), at pH 6.8 by 46% (**Figure 3B**), and at pH 7.4 by 76% (**Figure 3C**). It was also shown that the addition of chemically pure TEG at concentrations between 25 μM and 250 μM did not change the H_2O_2 concentration in the system, indicating that TEG does not have redox properties.

Thus, the modeling of oxidative stress by adding 1200 nM of H_2O_2 to 1 mM PBS showed that the CeNPs@TEG, at a concentration of 125 μM, inactivated up to 100% of the H_2O_2 introduced into the system. The results suggest that the pronounced antioxidant properties of CeNPs@TEG effectively protect biomolecules and tissues from the overproduction of H_2O_2 and ROS, the levels of which increase at the site of skin damage.

3.3. Cytotoxicity Study of CeNPs@TEG

The cytotoxicity of CeNPs@TEG was studied on HF and HaCaT cells after 24, 48, and 72 h of co-incubation. These cells were selected because they are key participants in the initiation, maintenance, and completion of wound healing. In addition, skin repair directly depends on the viability of fibroblasts and keratinocytes; therefore, the assessment of the cytotoxic effect on these cells is of considerable interest for subsequent *in vivo* experiments.[34]

Cellular NADP-H-dependent oxidoreductase activity and the viability of HF and HaCaT cells during the incubation with

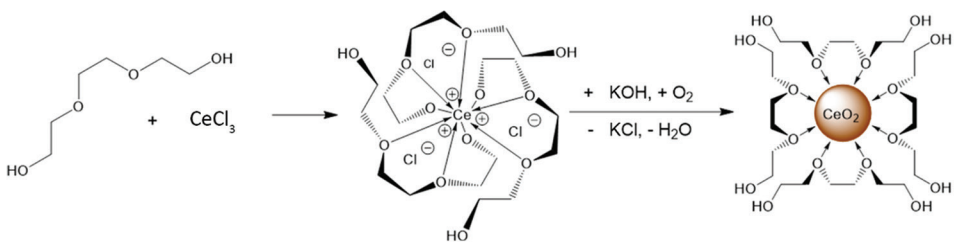

Figure 1. Schematic representation of the synthesis process and the proposed chemical structure of cerium oxide nanoparticles stabilized with triethylene glycol. The illustration was created using ChemDraw.

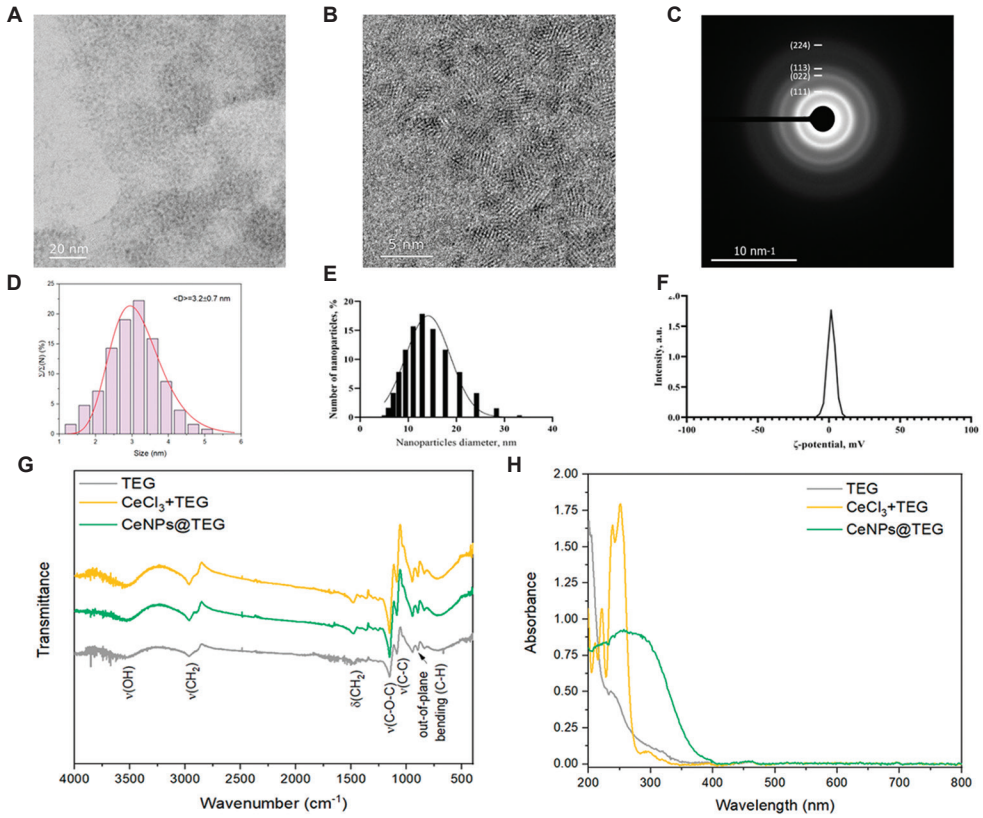

Figure 2. Investigation of the physicochemical properties of CeNPs@TEG. (A) TEM image of CeNPs@TEG. Scale bar: 20 nm; magnification: 300 kx. (B) TEM image of CeNPs@TEG. Scale bar: 5 nm; magnification: 1500 kx. (C) Electron diffraction pattern of CeNPs@TEG. (D) Size distribution of CeNPs@TEG measured by TEM. (E) Size distribution of CeNPs@TEG measured by dynamic light scattering. (F) ζ-potential distribution of CeNPs@TEG by electrophoretic light scattering. (G) Fourier transform infrared spectroscopy spectra. (H) Optical absorption spectra of the TEG, TEG with $CeCl_3$ solution, and CeNPs@TEG sol. . The illustration was created using Paint.NET.
Abbreviations: $CeCl_3$+TEG: A solution of cerium (III) chloride heptahydrate in triethylene glycol; CeNPs@TEG: Cerium oxide nanoparticles stabilized with triethylene glycol; TEM: Transmission electron microscope; TEG: Triethylene glycol.

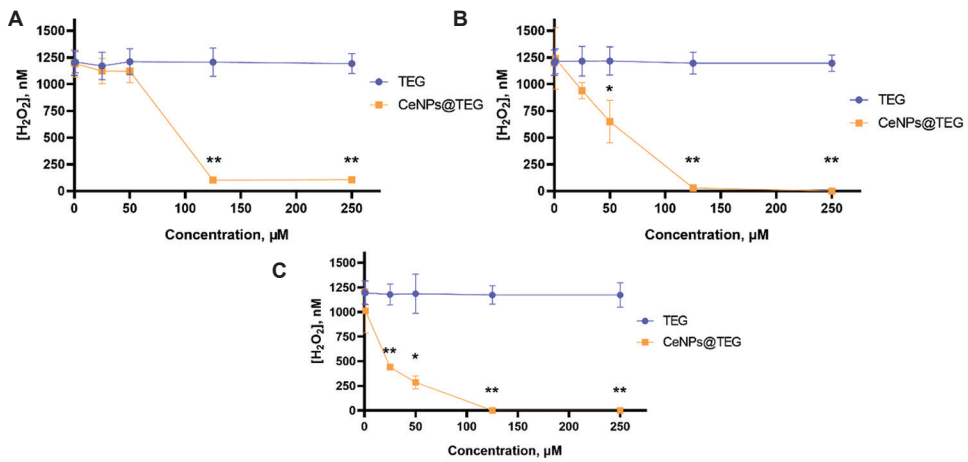

Figure 3. Antioxidant activity of CeNPs@TEG in aqueous solutions. The effect of CeNPs@TEG and TEG on various concentrations of exogenous H_2O_2 in 1 mM PBS at different pH values after 1 h of incubation (n = 10). (A) pH 5.5. (B) pH 6.8. (C) pH 7.4. Significant differences mean ± standard deviation compared using the Student's t-test, CeNPs@TEG vs. TEG. The illustration was created using GraphPad Prism 8.
Notes: *$0.01 \leq p < 0.05$, **$0.001 \leq p < 0.01$.
Abbreviations: CeNPs@TEG: Cerium oxide nanoparticles stabilized with triethylene glycol; TEG: Triethylene glycol.

CeNPs@TEG were evaluated in a concentration range from 25 μM to 1000 μM (**Figure 4**). It was found that there was no significant change in the activity of NADPH-dependent oxidoreductases of HF after 24- and 48-h incubation with CeNPs@TEG at concentrations ranging from 25 μM to 1000 μM compared to the activity of the intact control (**Figure 4A**). After 72 h of co-incubation of HF with CeNPs@TEG, the NADP-H-dependent oxidoreductase activity of the

cells decreased by 11–13% at concentrations between 50 and 500 μM. While at 25 and 1000 μM, no difference in metabolic activity was observed compared to the intact control group. The study of the oxidoreductase activity of HaCaT cells throughout the 72 h in the presence of CeNPs@TEG revealed a decline in the activity of NADPH-dependent oxidoreductases across the entire concentration range studied (**Figure 4B**). However, at a CeNPs@TEG concentration of 25 μM, the decrease in dehydrogenase activity was insignificant, amounting to < 10%.

The results of the live/dead assay showed that co-incubation of HF and HaCaT cells with CeNPs@TEG at concentrations ranging from 25 to 500 μM for 72 h did not increase the number of dead cells (**Figure 4C** and **D**). For HF cells, the proportion of dead cells remained below 4%, while for HaCaT, it was below 18%. This indicates the absence of any toxic effects from CeNPs@TEG at concentrations not exceeding 500 μM. However, when HaCaT cells were co-incubated with CeNPs@TEG at a concentration of 1000 μM, the proportion of dead cells increased to 61%, exceeding the half-maximal inhibitory concentration (IC_{50}) value.

Thus, the cytotoxicity study of CeNPs@TEG revealed that HaCaT cells were more sensitive to higher concentrations of CeNPs@TEG than HF. The IC_{50} of CeNPs@TEG for HaCaT was found to be 894 μM. For the HF cells, an IC_{50} value could not be determined within the tested concentration range, as no significant change in dehydrogenase activity or cell viability was observed with increasing CeNPs@TEG concentrations.

3.4. Investigation of the antioxidant properties of CeNPs@TEG in a H_2O_2-induced oxidative stress model *in vitro*

Hydrogen peroxide is a long-lived form of oxygen compared with other ROS, which makes it suitable for simulating oxidative stress induction *in vitro*.[9] The addition of exogenous H_2O_2 has been well described and widely used as a method for inducing oxidative stress in cell models.[35,36] Ransy *et al.*[37] showed that a concentration of H_2O_2 greater than 100 μM was needed to cause oxidative damage in cell models. In our study, we simulated oxidative stress by incubating HF and HaCaT cells for 60 min with 200 μM exogenous H_2O_2. Prior to adding H_2O_2, both cell lines were incubated with different concentrations of CeNPs@TEG (25–1000 μM) for 24 h.

The NADP-H-dependent oxidoreductase activity of HF and HaCaT cells in the Control+ group (without pre-incubation with CeNPs@TEG) differed after incubation with 200 μM H_2O_2 (**Figure 5A**). HF cells were more resistant to the effects of H_2O_2 compared with HaCaT. Adding 200 μM H_2O_2 to HF caused a 10% reduction in dehydrogenase activity, while adding the same amount of H_2O_2 to HaCaT resulted in a 38% decrease in NADPH-dependent oxidoreductase activity in the Control+ group. At the same time, pre-incubating HF with CeNPs@TEG at concentrations of 25 and 50 μM increased dehydrogenase activity by 8–10% compared to the Control+ group, corresponding to the NADP-H-dependent oxidoreductase activity in the Control– group (without H_2O_2 treatment). Pre-incubating HaCaT with CeNPs@TEG at concentrations ranging from 25 to 1000 μM had no effect on oxidoreductase activity, which remained at the level of the Control+ group.

The addition of exogenous H_2O_2 did not affect the viability of the HF cells (Control+ group). However, it increased the proportion of dead cells in the HaCaT cells (Control+ group) by 22% compared with the Control– group (**Figure 5B**). Due to the lack of significant differences between the Control– and Control+ groups, it was not possible to evaluate the antioxidant properties of CeNPs@TEG in this experiment for HF cells. At the same time, a preliminary 24-h incubation of HaCaT cells with CeNPs@TEG at concentrations ranging from 25 to 250 μM reduced the number of dead cells by 15–20%, whereas concentrations of 500 and 1000 μM, conversely, increased the number of dead cells compared to the Control+ group.

The study of the intracellular level of ROS showed that during the incubation of both cell cultures in the presence of

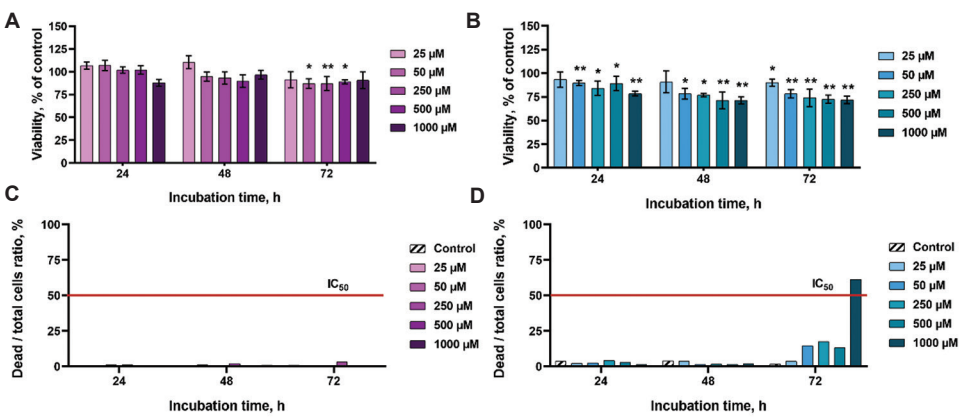

Figure 4. Investigation of cytotoxicity of CeNPs@TEG on HF and HaCaT cells. The NADP-H-dependent oxidoreductase activity of the cells after 24–72 h of co-incubation with CeNPs@TEG in concentrations from 25 to 1000 μM. (A) HF cells. (B) HaCaT cells. The data are presented as mean ± standard deviation via Welch's *t*-test. Live/dead assay results obtained after 24–72 h co-incubation with CeNPs@TEG in concentrations from 25 to 1000 μM. (C) HF cells. (D) HaCaT cells. The data are presented as meansmeans. The illustration was created using GraphPad Prism 8.
Notes: *$0.01 \le p < 0.05$, **$0.001 \le p < 0.01$.
Abbreviations: CeNPs@TEG: Cerium oxide nanoparticles stabilized with triethylene glycol; HaCaT: Human keratinocytes; HF: Human fibroblasts; NADP-H: Reduced form of nicotinamide adenine dinucleotide phosphate.

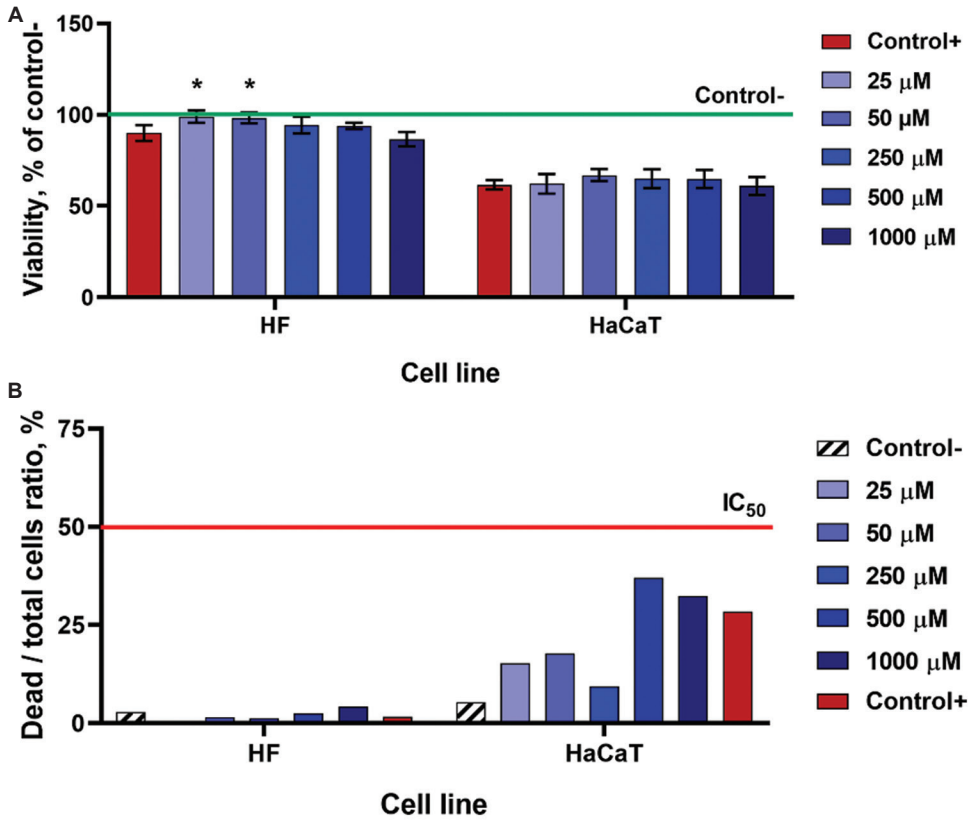

Figure 5. The effect of CeNPs@TEG on cell viability in a hydrogen peroxide-induced oxidative stress model. (A) Metabolic activity of HaCaT and HF after 24-h incubation with CeNPs@TEG at concentrations from 25 to 1000 μM before exposure to exogenous H_2O_2. Data are presented as mean ± standard deviation versus Control+ group through Welch's *t*-test. (B) Live/dead assay results obtained on HF and HaCaT after 24-h incubation with CeNPs@TEG at concentrations from 25 to 1000 μM before exposure to exogenous H_2O. The illustration was created using GraphPad Prism 8. Note: *0.01≤*p*<0.05.

Abbreviations: CeNPs@TEG: Cerium oxide nanoparticles stabilized with triethylene glycol; HaCaT: Human keratinocytes; HF: Human fibroblasts; IC_{50}: Half-maximal inhibitory concentration.

200 μM H_2O_2, there was an increase in ROS in the Control+ group, which was 30% for the HF cells and 40% for HaCaT, compared to the Control– group (**Figure 6**). Preliminary 24-h incubation of HF with CeNPs@TEG at concentrations of 25, 50, and 250 μM resulted in a decrease in ROS levels of 46%, 69%, and 45%, respectively, compared to the Control+ group. However, an increase in the CeNPs@TEG concentration to 500 μM resulted in ROS levels that remained at a level similar to the Control+ group, whereas an increase to 1000 μM caused an elevation in ROS levels in the HF culture by 97% compared to the Control+ group. Pre-incubation of HaCaT with CeNPs@TEG at concentrations ranging from 25 μM to 250 μM also led to a 75% reduction in ROS levels, but the maximum effective concentration was 500 μM, where the intracellular ROS level was 94% lower than the Control+ group.

It was demonstrated that CeNPs@TEG exhibited pronounced antioxidant properties under H_2O_2-induced oxidative stress in HF cells at a concentration of 25–50 μM. The most pronounced antioxidant effect was observed at a concentration of 50 μM, with a 70% reduction in intracellular ROS levels. Dehydrogenase activity and viability of HaCaT cells were unaffected by pre-incubation with CeNPs@TEG at the concentrations studied under H_2O_2-induced oxidative stress. However, pre-incubation of HaCaT cells with CeNPs@TEG at a concentration of 500 μM resulted in a 94% reduction in intracellular ROS compared to the Control+ group.

4. Discussion

Various synthesis methods are available for CeNPs, with the choice mainly determined by their intended biomedical application, such as wound healing, antioxidant therapy, or drug delivery, since different applications require specific particle sizes, morphologies, and surface characteristics.

Among widely used methods, alkaline precipitation in glycols, such as ethylene glycol, diethylene glycol, and TEG, has attracted attention. Conventional protocols involve a two-stage process: heating a $Ce(NO_3)_3{\cdot}6H_2O$ solution in glycol with aqueous ammonia at 75°C for 24 h, followed by dialysis to remove larger NPs and by-products. This often yields particles of ~40 nm, which are larger than desired, and requires extensive purification.[38]

Other approaches, such as sol–gel and hydrothermal synthesis, also have limitations. Sol–gel methods rely on hydrolysis and condensation, often require elevated temperatures and the use of organic solvents, which can result in aggregation and poor control over particle size and morphology.[39] Hydrothermal

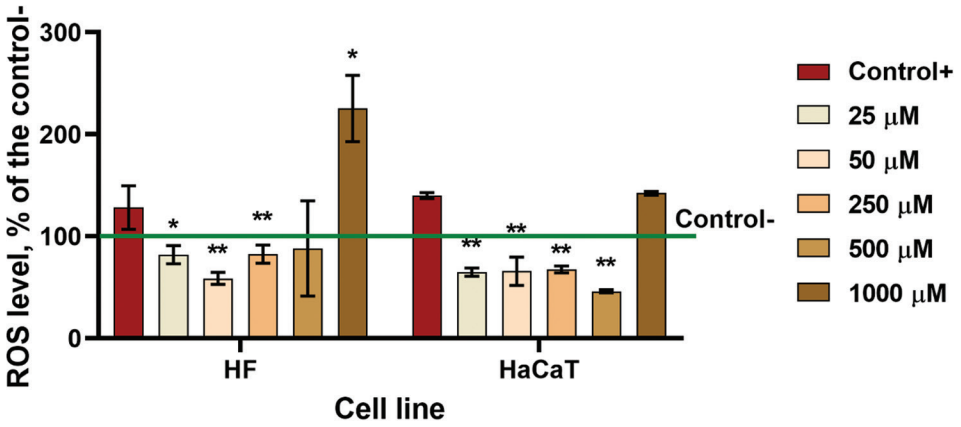

Figure 6. The effect of CeNPs@TEG on intracellular ROS level in a hydrogen peroxide-induced oxidative stress model. Intracellular ROS level of HF and HaCaT cells after 24-h co-incubation with CeNPs@TEG at concentrations from 25 to 1000 μM before exposure to exogenous H_2O_2. Data are presented as mean ± standard deviation vs. Control+ via Welch's *t*-test. The illustration was created using GraphPad Prism 8.
Notes: *$0.01 \leq p < 0.05$, **$0.001 < p < 0.01$.
Abbreviations: HaCaT: Human keratinocytes; HF: Human fibroblasts; ROS: Reactive oxygen species.

synthesis, while capable of producing uniform NPs, requires specialized equipment and strict parameter control; the resulting NPs produced may still exhibit broad size distributions and limited stability.[40]

Polyethylene glycol (PEG) is widely used to enhance dispersion and stability, but PEGylation usually involves post-synthesis modification and purification. In addition, PEG-coated particles may increase in size and form protein coronas, which can affect biocompatibility.[41] Surfactants can stabilize colloids but might also enlarge particles and reduce activity.[42,43] Polyols, such as TEG, are effective solvents because their viscosity prevents agglomeration, and excess amounts can rapidly reduce dissolved ions, leading to well-functionalized, stable NPs.[44-46] Moreover, their chelating ability regulates NP growth and aggregation, enhancing colloidal stability.[47,48] The one-step synthesis using TEG at 50°C proposed in this study enables the production of ultra-small CeNPs (3–5 nm) without surfactants. The only by-product is biologically compatible potassium chloride, and the sols obtained are highly stable, avoiding the formation of large particles or toxic impurities.

Our synthesis produced CeNPs@TEG with an average size of 3.2 ± 0.7 nm and a hydrodynamic diameter of 13 nm. The ζ-potential was close to zero, yet the sols remained stable for over 18 months, confirming that polyglycols provide long-term stability. Their ultra-small size suggests biological activity and low toxicity, supported by *in vitro* results. Importantly, such NPs can penetrate the stratum corneum, a valuable feature for medical applications.[25] The different responses of HF and HaCaT cells may be explained by their origin: HF is a primary cell culture, whereas HaCaT cells are immortalized. Primary cultures have a shorter lifespan, and evidence suggests that the results of cytotoxicity tests may vary depending on the number of passages.[49] However, primary cultures retain the original characteristics and genetic information of the parent organism. In contrast, immortalized cultures can undergo genetic changes that are not typical of primary cells. For instance, HaCaT has been shown to exhibit undesirable genetic alterations, including p53 mutations and an incorrect chromosome count,[50] as well as increased viability and apoptosis following exposure to gamma radiation.[51] Therefore, it is crucial to conduct cytotoxicity tests using different types of cell lines.

The strong antioxidant properties of CeNPs@TEG are attributed to the low ratio of $^{3+}$ and $^{4+}$ ions and the catalytic activity of CeNPs. While Ce^{3+} alone does not exhibit a full spectrum of antioxidant activity, CeNPs have been proven to deactivate most ROS and free radicals.[52,53] At the same time, the catalytic activity of CeNPs is thought to depend on the Ce^{4+} fraction.[54,55] In addition, the mimetic activity of phosphatase and superoxide dismutase enzymes in Ce^{4+} is much higher, and catalase-like activity is only found in a number of lanthanide compounds with an oxidation state of 4+.[25] This is important for mitigating oxidative stress in mechanical, thermal, autoimmune, and other skin injuries. Furthermore, studies have shown that the catalytic activity of CeNPs and the efficiency of the disproportionation process are influenced by the adsorption of H_2O_2 molecules onto the NPs' surface. This adsorption depends on the size of the NPs. Therefore, an increase in the surface area-to-volume ratio is considered to be the primary reason for the extraordinary catalytic activity of ultra-small CeNPs. As mentioned previously, glycol compounds, in particular TEG, can form complexes with lanthanides and thus regulate the growth of CeNPs and influence the level of oxygen non-stoichiometry in them.

While the current study provides valuable insights into the synthesis, physicochemical properties, and antioxidant activity of CeNPs@TEG, further investigations are necessary to fully elucidate their mechanisms of action at the cellular and molecular levels. In particular, detailed studies of gene expression and redox-sensitive signaling pathways would help clarify the regulatory processes influenced by CeNPs@TEG. In addition, more comprehensive analyses

of intracellular ROS dynamics using advanced fluorescent probes could provide critical information on the temporal and spatial effects of CeNPs@TEG under oxidative stress. Although the *in vitro* results are promising, *in vivo* studies are warranted to assess the biodistribution, pharmacokinetics, and therapeutic efficacy of CeNPs@TEG in complex biological systems, particularly in models of skin injury or oxidative damage.

5. Conclusions

The synthesized CeNPs@TEG exhibited pronounced antioxidant properties due to the presence of CeNPs. Since persistent oxidative stress and excessive ROS production are key factors in the pathogenesis of skin damage, blocking the action of harmful molecules or deactivating ROS using CeNPs@TEG offers a promising approach for treating various types of skin damage, including those caused by mechanical, thermal, and radiation damage.

Acknowledgement

We would like to express our gratitude to E. E. Karmanova (Institute of Cell Biophysics of the Russian Academy of Sciences) for methodological assistance in measuring the antioxidant activity of CeNPs@TEG by enhanced chemiluminescence. The research was carried out using equipment from Moscow State University (MSU) Shared Research Equipment Centre, "Technologies for obtaining new nanostructured materials and their complex study," acquired under the MSU Equipment Renovation Program (National Project "Science") and the MSU Program of Development.

Financial support

This study was supported by the Russian Science Foundation (No. 22-63-00082).

Conflicts of interest statement

The authors declare no conflicts of interest.

Author contributions

Conceptualization: NRP; *Data curation:* VAA; *Formal analysis:* DAK; *Methodology*: ALP; *Investigation*: VAA; *Project administration*: ALP and EAZ; *Supervision:* NRP; *Visualization:* VAA; *Writing—original draft*: VAA; *Writing—review & editing:* EAZ and NRP. All authors have read and agreed to the published version of the manuscript.

Ethics approval and consent to participate

Not applicable.

Consent for publication

Not applicable.

Availability of data

The authors confirm that the data supporting the findings of this study are available within the article. Raw data that support the findings of this study are available from the corresponding authors upon reasonable request.

References

1. Dunnill C, Patton T, Brennan J, *et al.* Reactive oxygen species (ROS) and wound healing: The functional role of ROS and emerging ROS-modulating technologies for augmentation of the healing process. *Int Wound J.* 2015;14(1):89-96. doi: 10.1111/iwj.12557
2. Polaka, S, Katare, P, Pawar, B, *et al.* Emerging ROS-modulating technologies for augmentation of the wound healing process. *ACS Omega.* 2022;7(35):30657-30672. doi: 10.1021/acsomega.2c02675
3. Canton, M, Sánchez-Rodríguez, R, Spera, I, *et al.* Reactive oxygen species in macrophages: Sources and targets. *Front Immunol.* 2021;12:734229. doi: 10.3389/fimmu.2021.734229
4. Sipka T, Peroceschi R, Hassan-Abdi R, *et al.* Damage-induced calcium signaling and reactive oxygen species mediate macrophage activation in zebrafish. *Front Immunol.* 2021;12:636585. doi: 10.3389/fimmu.2021.636585.
5. Wang G, Yang F, Zhou W, Xiao N, Luo M, Tang Z. The initiation of oxidative stress and therapeutic strategies in wound healing. *Biomed Pharmacother.* 2023;157:114004. doi: 10.1016/j.biopha.2022.114004
6. Armstrong DG, Jude EB. The role of matrix metalloproteinases in wound healing. *J Am Podiatr Med Assoc.* 2002;92(1):12-18. doi: 10.7547/87507315-92-1-12
7. Dissemond J, Goos M, Wagner SN. The role of oxidative stress in the pathogenesis and therapy of chronic wounds. *Hautarzt.* 2002;53(11):718-723. doi: 10.1007/s00105-001-0325-5
8. Janko M, Ontiveros F, Fitzgerald TJ, Deng A, DeCicco M, Rock KL. IL-1 generated subsequent to radiation-induced tissue injury contributes to the pathogenesis of radiodermatitis. *Radiat Res.* 2012;178(3):166-172. doi: 10.1667/RR3097.1
9. Robbins MEC, Zhao W. Chronic oxidative stress and radiation-induced late normal tissue injury: A review. *Int J Radiat Biol.* 2004;80(4):251-259. doi: 10.1080/09553000410001692726
10. McBride WH, Chiang CS, Olson JL, *et al.* A sense of danger from radiation. *Radiat Res.* 2004;162(1):1-19. doi: 10.1667/rr3196
11. Valko M, Leibfritz D, Moncol J, Cronin MTD, Mazur M, Telser J. Free radicals and antioxidants in normal physiological functions and human disease. *Int J Biochem Cell Biol.* 2007;39(1):44-84. doi: 10.1016/j.biocel.2006.07.001
12. Hu SCS, Hou MF, Luo KH, *et al.* Changes in biophysical properties of the skin following radiotherapy for breast cancer. *J Dermatol.* 2014;41(12):1087-1094. doi: 10.1111/1346-8138.12669
13. Bray FN, Simmons BJ, Wolfson AH, Nouri K. Acute and chronic cutaneous reactions to ionizing radiation therapy. *Dermatol Ther (Heidelb).* 2016;6(2):185-206. doi: 10.1007/s13555-016-0120-y
14. Anikina VA, Sorokina SS, Shemyakov AE, *et al.* An experimental model of proton-beam-induced radiation dermatitis *in vivo*. *Int J Mol Sci.* 2023;24(22):16373. doi: 10.3390/ijms242216373
15. Popova NR, Andreeva VV, Khohlov NV, Popov AL, Ivanov VK. Fabrication of CeO2 nanoparticles embedded in polysaccharide hydrogel and their application in skin wound healing. *Nanosystems Phys Chem Math.* 2020;11(1):99-109. doi: 10.17586/2220-8054-2020-11-1-99-109
16. Comino-Sanz IM, López-Franco MD, Castro B, Pancorbo-Hidalgo PL. The role of antioxidants on wound healing: A review of the current evidence. *J Clin Med.* 2021;10(16):3558. doi: 10.3390/jcm10163558
17. Shcherbakov AB, Reukov VV, Yakimansky AV, *et al.* CeO_2 nanoparticle-containing polymers for biomedical applications: A review. *Polymers (Basel).* 2021;13(6):924. doi: 10.3390/polym13060924
18. Popov Anton L, Khohlov Nikolai V, Popova Nelli R, *et al.* Composite cerium oxide nanoparticles - containing polysaccharide hydrogel as effective agent for burn wound healing. *Key Eng Mater.* 2021;899:493-505. doi: 10.4028/www.scientific.net/KEM.899.493
19. Xue Y, Luan Q, Yang D, Yao X, Zhou K. Direct evidence for hydroxyl radical scavenging activity of cerium oxide nanoparticles. *J Phys Chem C.* 2011;115(11):4433-4438. doi: 10.1021/jp109819u
20. Wu Y, Ta HT. Different approaches to synthesising cerium oxide nanoparticles and their corresponding physical characteristics, and

ROS scavenging and anti-inflammatory capabilities. *J Mater Chem B.* 2021;9(36):7291-7301.
doi: 10.1039/d1tb01091c

21. Plakhova TV, Romanchuk AY, Butorin SM, *et al.* Towards the surface hydroxyl species in CeO_2 nanoparticles. *Nanoscale.* 2019;11(39):18142-18149.
doi: 10.1039/c9nr06032d
22. Barker E, Shepherd J, Asencio IO. The use of cerium compounds as antimicrobials for biomedical applications. *Molecules.* 2022;27(9):2678.
doi: 10.3390/molecules27092678.
23. Popova NR, Shekunova TO, Popov AL, Selezneva II, Ivanov VK. Cerium oxide nanoparticles provide radioprotective effects upon X-ray irradiation by modulation of gene expression. *Nanosyst Phys Chem Math.* 2019;10(5):564-572.
doi: 10.17586/2220-8054-2019-10-5-564-572
24. Popov AL, Andreeva VV, Khohlov NV, Kamenskikh KA, Gavrilyuk VB, Ivanov VK. Comprehensive cytotoxicity analysis of polysaccharide hydrogel modified with cerium oxide nanoparticles for wound healing application. *Nanosys Phys Chem Math.* 2021;12(3):329-335.
doi: 10.17586/2220-8054-2021-12-3-329-335
25. Shcherbakov AB, Zholobak NM, Ivanov VK. Biological, Biomedical and Pharmaceutical Applications of Cerium Oxide. In: Scirè S, Palmisano L, editors. *Cerium Oxide (CeO_2): Synthesis, Properties and Applications.* Ch. 8. Metal Oxides; Elsevier; 2020. p. 279-358.
doi: 10.1016/B978-0-12-815661-2.00008-6
26. Kannan S, Sundrarajan M. A green approach for the synthesis of a cerium oxide nanoparticle: Characterization and antibacterial activity. *Int J Nanosci.* 2014;13:1450018.
doi: 10.1142/S0219581X14500185
27. Pulido-Reyes G, Rodea-Palomares I, Das S, *et al.* Untangling the biological effects of cerium oxide nanoparticles: The role of surface valence states. *Sci Rep.* 2015;5(1):15613.
doi: 10.1038/srep15613
28. Ballantyne B, Snellings WM. Triethylene glycol HO(CH2CH2O)3H. *J Appl Toxicol.* 2007;27(3):291-299.
doi: 10.1002/jat.1220
29. Doan VN, Hung VQ, Son PN, *et al.* Synthesis, characterization, and antimicrobial activity of a lanthanum complex with a triethylene glycol Ligand. *Inorg Chim Acta.* 2023;556:121637.
doi: 10.1016/j.ica.2023.121637
30. Yu HL, Goh CF. Glycols: The ubiquitous solvent for dermal formulations. *Eur J Pharm Biopharm.* 2024;196:114182.
doi: 10.1016/j.ejpb.2024.114182
31. Duggan K, Ijaz MK, McKinney J, Maillard JY. Reviewing the evidence of antimicrobial activity of glycols. *J Appl Microbiol.* 2024;135(4):lxae071.
doi: 10.1093/jambio/lxae071
32. Bruskov VI. Heat-induced formation of reactive oxygen species and 8-oxoguanine, a biomarker of damage to DNA. *Nucleic Acids Res.* 2002;30(6):1354-1363.
doi: 10.1093/nar/30.6.1354
33. Karmanova EE, Chernikov AV, Popova NR, Sharapov MG, Ivanov VE, Bruskov VI. Metformin mitigates radiation toxicity exerting antioxidant and genoprotective properties. *Naunyn Schmiedebergs Arch Pharmacol.* 2023;396(10):2449-2460.
doi: 10.1007/s00210-023-02466-w
34. Wilson JR, Mills JG, Prather ID, Dimitrijevich SD. A toxicity index of skin and wound cleansers used on *in vitro* fibroblasts and keratinocytes. *Adv Skin Wound Care.* 2005;18(7):373-378.
doi: 10.1097/00129334-200509000-00011
35. Ward JF, Evans JW, Limoli CL, Calabro-Jones PM. Radiation and hydrogen peroxide induced free radical damage to DNA. *Br J Cancer Suppl.* 1987;8:105-112.
36. Coyle CH, Martinez LJ, Coleman MC, Spitz DR, Weintraub NL, Kader KN. Mechanisms of H_2O_2-induced oxidative stress in endothelial cells. *Free Radic Biol Med.* 2006;40(12):2206-2213.
doi: 10.1016/j.freeradbiomed.2006.02.017
37. Ransy C, Vaz C, Lombès A, Bouillaud F. Use of H_2O_2 to cause oxidative stress, the catalase issue. *Int J Mol Sci.* 2020;21(23):9149.
doi: 10.3390/ijms21239149
38. Uekawa N, Yoshida K, Kobayashi M, Kojima T. Synthesis of cerium oxide (IV) stable sol using the dialysis process of glycol solution of cerium nitrate hydrate. *J Sol Gel Sci Technol.* 2020;93(1):91-99.
doi: 10.1007/s10971-019-05155-4
39. Hosseini M, Amjadi I, Mohajeri M, Mozafari M. Sol-Gel synthesis, physico-chemical and biological characterization of cerium oxide/polyallylamine nanoparticles. *Polymers.* 2020;12(7):1444.
doi: 10.3390/polym12071444
40. Exposito AJ, Barrie PJ, Torrente-Murciano L. Fast synthesis of CeO_2 nanoparticles in a continuous microreactor using deep eutectic reline as solvent. *ACS Sustain Chem Eng.* 2020;8(49):18297-18302.
doi: 10.1021/acssuschemeng.0c06949
41. Xue Y, Balmuri SR, Patel A, Sant V, Sant S. Synthesis, physico-chemical characterization, and antioxidant effect of PEGylated cerium oxide nanoparticles. *Drug Deliv Transl Res.* 2018;8(2):357-367.
doi: 10.1007/s13346-017-0396-1
42. Bastami TR, Entezari MH. High stable suspension of magnetite nanoparticles in ethanol by using sono-synthesized nanomagnetite in polyol medium. *Mater Res Bull.* 2013;48(9):3149-3156.
doi: 10.1016/j.materresbull.2013.04.067
43. Parveen R, Ullah S, Sgarbi R, Tremiliosi-Filho G. One-pot ligand-free synthesis of gold nanoparticles: The role of glycerol as reducing-cum-stabilizing agent. *Colloid Surf A Physicochem Eng Aspects.* 2019;565:162-171.
doi: 10.1016/j.colsurfa.2019.01.005
44. Quinson J, Nielsen TM, Escudero-Escribano M, Jensen KMØ. Room temperature syntheses of surfactant-free colloidal gold nanoparticles: The benefits of mono-alcohols over polyols as reducing agents for electrocatalysis. *Colloid Surf A Physicochem Eng Aspects.* 2023;675:131853.
doi: 10.1016/j.colsurfa.2023.131853
45. Dong H, Chen YC, Feldmann C. Polyol synthesis of nanoparticles: Status and options regarding metals, oxides, chalcogenides, and non-metal elements. *Green Chem.* 2015;17(8):4107-4132.
doi: 10.1039/C5GC00943J
46. Tang X, Choo ESG, Li L, Ding J, Xue J. One-pot synthesis of water-stable ZnO nanoparticles via a polyol hydrolysis route and their cell labeling applications. *Langmuir.* 2009;25(9):5271-5275.
doi: 10.1021/la900374b
47. Wang Y, Ren J, Deng K, Gui L, Tang Y. Preparation of tractable platinum, rhodium, and ruthenium nanoclusters with small particle size in organic media. *Chem Mater.* 2000;12(6):1622-1627.
doi: 10.1021/cm0000853
48. Fiévet F, Ammar-Merah S, Brayner R, *et al.* The polyol process: A unique method for easy access to metal nanoparticles with tailored sizes, shapes and compositions. *Chem Soc Rev.* 2018;47(14):5187-5233.
doi: 10.1039/C7CS00777A
49. Boonkaew B, Kempf M, Kimble R, Cuttle L. Cytotoxicity testing of silver-containing burn treatments using primary and immortal skin cells. *Burns.* 2014;40(8):1562-1569.
doi: 10.1016/j.burns.2014.02.009
50. Choi M, Park M, Lee S, *et al.* Establishment of immortalized primary human foreskin keratinocytes and their application to toxicity assessment and three dimensional skin culture construction. *Biomol Ther (Seoul).* 2017;25(3):296-307.
doi: 10.4062/biomolther.2017.043
51. Petit-Frere C, Capulas E, Lyon DA, *et al.* Apoptosis and cytokine release induced by ionizing or ultraviolet B radiation in primary and immortalized human keratinocytes. *Carcinogenesis.* 2000;21(6):1087-1095.
52. Schubert D, Dargusch R, Raitano J, Chan SW. Cerium and yttrium oxide nanoparticles are neuroprotective. *Biochem Biophys Res Commun.* 2006;342(1):86-91.
doi: 10.1016/j.bbrc.2006.01.129
53. Singh KR, Nayak V, Sarkar T, Singh RP. Cerium oxide nanoparticles: Properties, biosynthesis and biomedical application. *RSC Adv.* 2020;10(45):27194-27214.
doi: 10.1039/d0ra04736h
54. Zholobak NM, Shcherbakov AB, Bogorad-Kobelska AS, *et al.* Panthenol-stabilized cerium dioxide nanoparticles for cosmeceutic formulations against ROS-induced and UV-induced damage. *J Photochem Photobiol B Biol.* 2014;130:102-108.

doi: 10.1016/j.jphotobiol.2013.10.015

55. Popov AL, Popova NR, Selezneva II, Akkizov AY, Ivanov VK. Cerium oxide nanoparticles stimulate proliferation of primary mouse embryonic fibroblasts *in vitro*. *Mater Sci Eng C Mater Biol Appl.* 2016;68:406-413. doi: 10.1016/j.msec.2016.05.103

Received: May 26, 2025
Revised: September 19, 2025
Accepted: October 9, 2025
Available online: November 10, 2025